Mater. Res. Soc. Symp. Proc. Vol. 1217 © 2010 Materials Research Society 1217-Y01-04

Monodisperse Pt-Cu Nanocubes: Synthesis, Characterization, and Electrochemical Properties

Dan Xu[1], Hongzhou Yang[2], Shouzhong Zou[2] and Jiye Fang[1,*]
[1]Department of Chemistry, State University of New York at Binghamton, Binghamton, New York 13902
[2]Department of Chemistry and Biochemistry, Miami University, Oxford, Ohio 45056

ABSTRACT

High-quality Pt-Cu nanocubes were prepared through simultaneous reduction of platinum (II) acetylacetonate and copper (Π) acetylacetonate in 1-octadecene by 1,2–tetradecanediol in the presence of tetraoctylammonium bromide, oleylamine, and 1-dodecanethiol. The growth process of Pt-Cu nanocubes was explored based on the observation of intermediates. The electrocatalytic behavior indicates that cubic Pt-Cu nanocrystals are more active than spherical Pt-Cu nanocrystals and Pt nanocrystals towards methanol oxidation reaction.

INTRODUCTION

Platinum (**Pt**) nanoparticles (**NPs**) have been the subject of extensive studies because of their unique catalytic properties in various significant applications[1-5]. It has been realized that the catalytic activity of Pt NPs highly depends on the surface atomic arrangements on a particle.[6-8] For example, electrochemical evaluation on oxygen reduction reaction (**ORR**) in adsorbing acidic solutions indicates that Pt {100} are more active than Pt {111} planes [9, 10]. As electrocatalysts, nanocubes (**NCbs**) of Pt [11-13] therefore receive more interest than other morphologies such as multipod[14, 15] and one-dimensional nanostructure[16, 17]. In order to reduce the overall use of expensive Pt, Pt-based bimetallic nanocrystals (**NCs**) such as Pt-Ni[18, 19], Pt-Co[20-22], and Pt-Cu[23-25] have attracted an increasing interest as well. Moreover, recent reports indicate that electrocatalytic activities of some Pt-bimetallic NCs are superior to those of pure Pt metal[26, 27]. Therefore, it is highly worthwhile and significant to synthesize the Pt-bimetallic NCbs and to examine their electrocatalytic performance. To the best of our knowledge, however, there have been very few reports on preparation of Pt-bimetallic NCbs and examination of their electrocatalytic performances to date. In this paper, we report the studies on growth mechanism of Pt-Cu NCbs and comparison of the electrocatalytic activities towards methanol oxidation reaction among spherical Pt, Pt-Cu NPs and Pt-Cu NCbs.

EXPERIMENT

Synthesis of Pt-Cu nanocubes.

The synthesis was carried out using a standard airless procedure. For a typical synthesis, 0.05 mmol of platinum (II) acetylacetonate [**Pt**(**acac**)$_2$], 0.05 mmol of copper (II) acetylacetonate [**Cu**(**acac**)$_2$], 0.5 mmol of 1,2–tetradecanediol (**TDD**) and 0.6 mmol of tetraoctylammonium bromide (**TOAB**) were mixed in 7.0 ml 1-octadecene (**ODE**). The mixture was then heated to 110 ^{o}C with vigorous stirring followed by a subsequent injection of 1.6 ml of pre-prepared

oleylamine (**OLA**) in ODE (0.94 mmol for OLA) and 0.25 ml of pre-prepared 1-dodecanethiol ($C_{12}SH$, **DDT**) in ODE (0.05 mmol for $C_{12}SH$). The clear yellowish mixture was continually heated to 230 ^{o}C and then maintained for 20 min. Toluene was used to quench the reaction and remove the excessive surfactants when the reaction finished and temperature dropped to 200 ^{o}C. The resultant NCs were isolated by adding a sufficient amount of anhydrous ethanol followed by centrifugation at 4100 *rpm* for 8 min. The product was then re-dispersed in anhydrous hexane for further characterization.

Synthesis of spherical Pt-Cu nanocrystals.

Spherical PtCu NCs were synthesized using the same procedure of Pt-Cu NCbs in the absence of TOAB.

Synthesis of spherical Pt nanocrystals.

0.5 mmol of $Pt(acac)_2$, 10 mL of benzyl ether, 1.0 mL OLA and 1.0 mL of oleic acid were mixed in a three-neck flask and heated to 120 °C for 20 min under argon protection. Temperature was then increased to 200 °C and remained for 30 min before the system was cooled down. The products were separated by adding excessive amount of anhydrous ethanol followed by centrifugation. The isolated Pt NCs were re-dispersed in anhydrous hexane, producing a colloidal suspension.

Characterizations

The X-ray diffraction (**XRD**) data of the samples were collected on a PANanalytical X-ray diffractometer (X'Pert system) equipped with a Cu Kα1 radiation source (λ = 0.15406 nm). TEM images were obtained from a Hitachi 7000 transmission electron microscope. A JEOL-2010 FEG TEM was used for high-resolution transmission electron microscopy (**HRTEM**) imaging, selected-area electron diffraction (**SAED**), and energy dispersive X-ray spectroscopic (**EDS**) data collection on Ni TEM sample grids. Electrochemical studies were conducted using a CHI 700B electrochemical analyzer (CH Instruments, Austin, TX) with a two-compartment, three-electrode glass cell. A Ag/AgCl electrode saturated with KCl solution was used as the reference electrode and a Pt wire as the counter electrode. To prepare a catalyst coated GC electrode, 4.0 μL of the NP colloidal suspension in hexane was spin-coated on a polished glassy carbon (**GC**) electrode. The NP-coated GC electrode was then subjected to Ar plasma cleaning for 10 min to remove the residues of high boiling point organic species. Methanol oxidation voltammograms and chronoamperometric experiments were carried out in 0.1 M $HClO_4$ + 1 M MeOH solution. All electrolyte solutions were prepared using Milli-Q water with a resistivity of 18.2 MΩ cm^{-1}. All of the electrochemical evaluations were conducted at room temperature (23±1 °C).

RESULTS AND DISCUSSION

TEM characterizations of Pt-Cu nanocrystals

Figure 1 shows typical transmission electron microscopic (TEM) images of the as-prepared Pt-Cu NCbs. The overall morphology of the sample, as shown in Figure 1a,

demonstrates that most of the NPs display in cubic morphology with side length of about 8.0 nm. Figure 1b is a HRTEM image of arrays of Pt-Cu NCbs with sharp corners, indicating the high crystallinity of those NCbs.

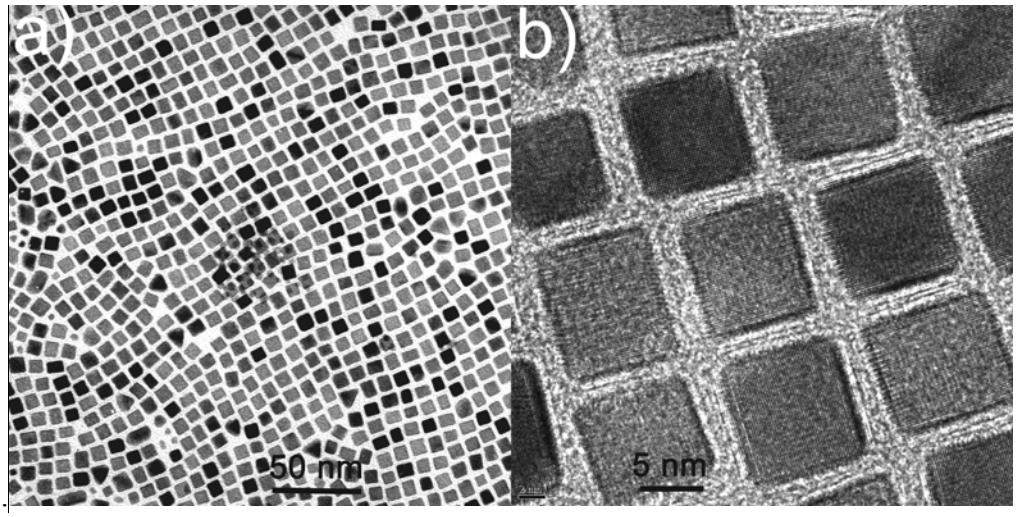

Figure 1. (a) Low magnification TEM image of Pt-Cu nanocubes; (b) High resolution TEM image of arrays of Pt-Cu nanocubes.

XRD and TEM-EDS characterizations of Pt-Cu nanocubes

Figure 2a shows a typical XRD pattern of the sample suspension deposited on a polished <100> silicon wafer, displaying the typical peaks which are in agreement with those of a standard PtCu pattern (refer to JCPDS ICDD card 48-1549). The tremendously stronger intensity of the 200 diffraction peak than that of the 111 peak indicates that the NC pattern is (100) textured. The alloy composition was evaluated using a TEM-EDS. The average molar ratio of Pt/Cu of the alloy is 6.0:4.0 (± 0.02). One of the EDS spectra is shown in Figure 2b.

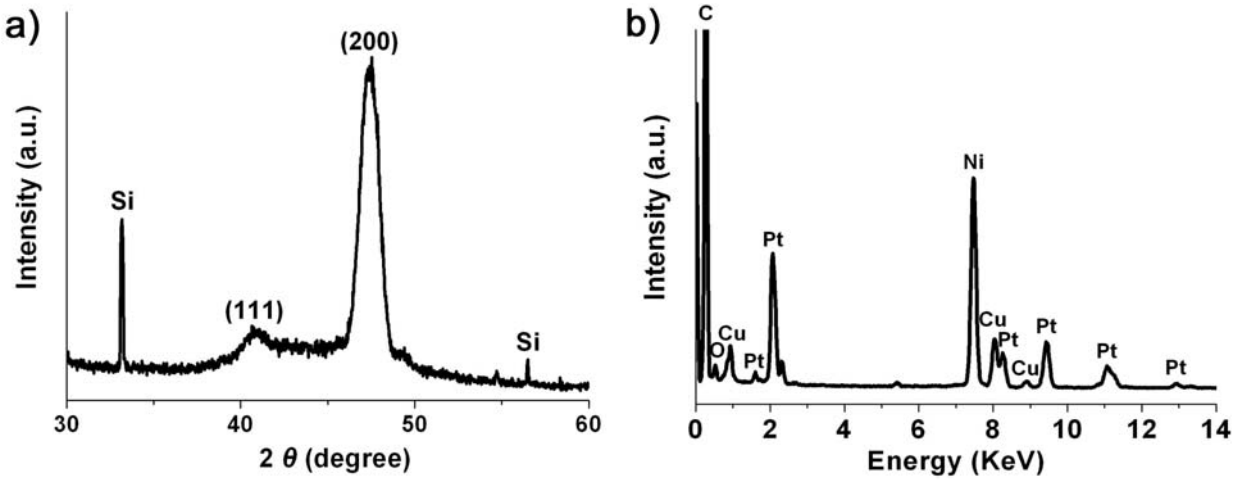

Figure 2. (a) X-ray diffraction (XRD) pattern of a self-assembled thin film of Pt-Cu nanocubes; (b) TEM-EDS spectrum of Pt-Cu nanocubes.

Growth mechanism of Pt-Cu nanocubes

To explore the NCbs growth mechanism, we collected the intermediate by precisely tuning the relative amount of TDD and DDT. Figure 3a shows a TEM image of the instantaneous product while the color of the solution quickly changes from light-yellow to dark-brown, which is believed to be the intermediate while the formed nucleating seeds were converting to the NCbs. As illustrated, most of the NCs (>90%) are octapods with a size range of 7-8 nm, and some are tetrahedral NCs. It has been reported that NC evolution consists of a nucleation stage followed by a further Ostwald ripening growth [28, 29]. For an fcc structure, it is well known that {100} crystallographic facets generally possess higher surface energy than {111} do [30, 31]. In order to minimize the total surface energy, the tiny nucleating seeds tend be developed as octapods/tetrahedra structure which is bounded by {111} low-surface-energy facets. When the seeds are completely generated, the further growth of NCs will be thermodynamically dominated by the combination influences of mixed capping ligands through the consumption of feedstock in solution. In our case, the continually reduced Pt and Cu atoms will be energetically favorable for filling into the spaces between the octapods branches and therefore the NPs will eventually develop into solid cubes. It is worth mentioning that the process of Pt-Cu NCs nucleation and additional growth is actually pretty fast. Under present conditions, it only needs around 4 min to develop into “crepe-shaped” Pt-Cu NCbs, as illustrated in Figure 3b.

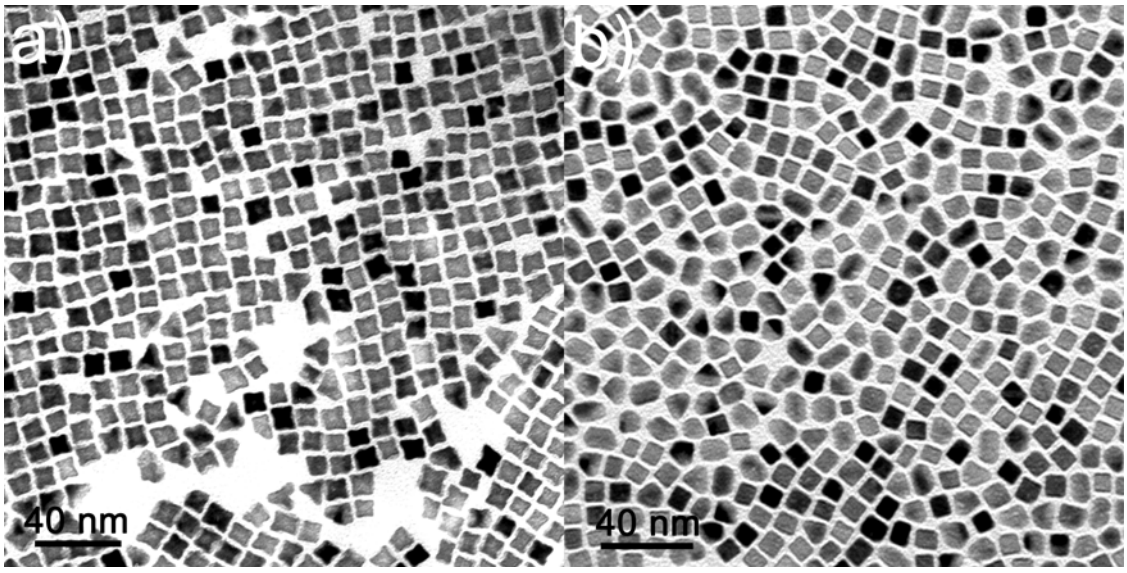

Figure 3. TEM images of intermediate products. (a) During the solution color-change from light yellow to dark brown (TDD: 0.25 mmol; DDT: 0.07 mmol); (b) after 4 min at 230 °C (TDD: 0.5 mmol; DDT: 0.05 mmol).

Electrochemical properties of Pt-Cu nanocubes

Figure 4a illustrates a cyclic voltammograms (**CV**) of these cubic Pt-Cu, spherical Pt-Cu and Pt NCs with similar sizes in 0.1 M $HClO_4$ + 1 M MeOH. The current density was calculated with respect to the Pt surface area measured from the hydrogen adsorption/desorption charges. As shown in Figure 4a, Pt-Cu NCbs show the highest methanol oxidation current density. Higher methanol oxidation activity of cubic Pt-Cu NCs was further confirmed by the

chronoamperometric measurements performed at 0.8 V (Figure 4b). As can be appreciated, the catalytic activity towards methanol oxidation follows the order, cubic Pt-Cu NCs > spherical Pt-Cu NCs > spherical Pt NCs. It is worth to note that the methanol oxidation activity of spherical Pt-Cu NCs decreases at longer period of time, and eventually reaches the same level as that of spherical Pt NCs.

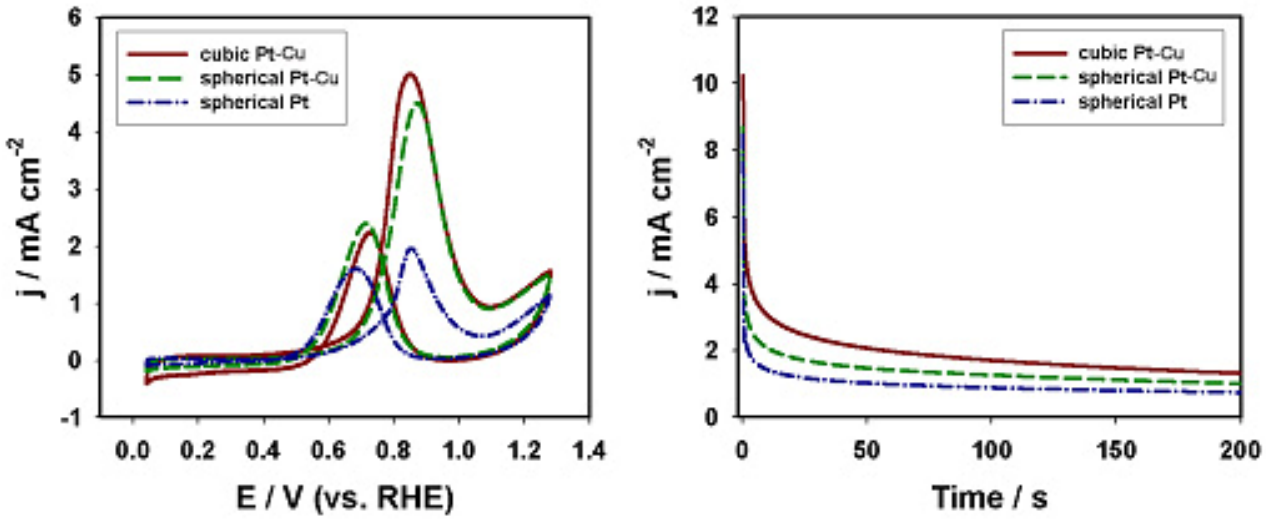

Figure 4. (a) Cyclic voltammograms of MeOH oxidation on Pt-Cu nanocubes, Pt-Cu nanospheres and Pt nanospheres in 0.1 M $HClO_4$ + 1.0 M MeOH (Scan rate: 0.02 V s^{-1}); (b) Chronoamperometric results of MeOH oxidation at 0.8 V on Pt-Cu nanocubes, Pt-Cu nanospheres and Pt nanospheres in 0.1 M $HClO_4$ + 1.0 M MeOH.

CONCLUSIONS

In summary, monodisperse Pt-Cu NCbs were successfully prepared through an effective colloidal method. The mechanism of those Pt-Cu NCbs nucleation and growth was accordingly discussed based on the observation of intermediate NPs by precisely controlling the reaction parameters. Electrochemical catalytic activities of Pt-Cu NCbs, Pt-Cu nanospheres as well as Pt nanospheres with similar sizes towards methanol oxidation reaction were also comparatively studied. The electrochemical evaluation results indicate that the {100}-terminated Pt-Cu NCbs exhibit a superior electrocatalytic activity towards methanol oxidation reaction in comparison with those of spherical Pt-Cu NCs and Pt NCs. Such shape-controlled nanomaterials with notable electrocatalytic performance could be regarded as promising anode catalysts in the fuel cell industry.

ACKNOWLEDGMENTS

This work was supported by NSF (DMR-0731382 & CHM-0616436) and Binghamton University. We thank Dr. Amar Kumbhar for his help in observing HRTEM images and Dr. Qingsheng Liu for his help in composition analysis.

REFERENCES

1. R. Narayanan, M. A. El-Sayed, *J. Phys. Chem. B*, **107**, 12416-12424 (2003).
2. J. Zhang, M. B. Vukmirovic, Y. Xu, M. Mavrikakis, R. R. Adzic, *Angew. Chem. Int. Ed.* **44**, 2132-2135 (2005).
3. M. S. El-Deab, T. Ohsaka, *Angew. Chem. Int. Ed.* **45**, 5963-5966 (2006).
4. A. T. Bell, *Science* **299**, 1688-1691 (2003).
5. A. Roucoux, J. Schulz, H. Patin, *Chem. Rev.* **102**, 3757-3778 (2002).
6. R. Narayanan, M. A. El-Sayed, *J. Am. Chem. Soc.* **126**, 7194-7195 (2008).
7. N. Tian, Z.-Y. Zhou, S.-G. Sun, Y. Ding, Z. L. Wang, *Science* **316**, 732-735 (2007).
8. R. Narayanan, M. A. El-Sayed, *Nano. Lett.* **4**, 1343-1348 (2004).
9. N. M. Markovic, H. A. Gasteiger, J. Philip N. Ross, *J. Phys. Chem.* **99**, 3411-3415 (1995).
10. K. Kinoshita, *J. Electrochem. Soc.* **137**, 845-848 (1990).
11. H. Lee, S. E. Habas, S. Kweskin, D. Butcher, G. A. Somorjai, P. Yang, *Angew. Chem. Int. Ed.* **45**, 7824-7828 (2006).
12. H. Song, F. Kim, S. Connor, G. A. Somorjai, P. Yang, *J. Phys. Chem. B* **109**, 188-193 (2005).
13. T. S. Ahmadi, Z. L. Wang, T. C. Green, A. Henglein, M. A. El-Sayed, *Science* **272**, 1924-1925 (1996).
14. X. Teng, H. Yang, *Nano. Lett.* **5**, 885-891 (2005).
15. J. Chen, T. Herricks, Y. Xia, *Angew. Chem. Int. Ed.* **44**, 2589-2592 (2005).
16. B. Mayers, X. Jiang, D. Sunderland, B. Cattle, Y. Xia, *J. Am. Chem. Soc.* **125**, 13364-13365 (2003).
17. J. Chen, T. Herricks, M. Geissler, Y. Xia, *J. Am. Chem. Soc.* **126,** 10854 -10855 (2004).
18. T. Jacob, W. A. G. III, *J. Phys. Chem. B* **108,** 8311-8323 (2004).
19. K.-W. Park, J.-H. Choi, B.-K. Kwon, S.-A. Lee, Y.-E. Sung, H.-Y. Ha, S.-A. Hong, H. Kim, A. Wieckowski, *J. Phys. Chem. B* **106,** 1869-1877 (2002).
20. Z. Liu, C. Yu, I. A. Rusakova, D. Huang, P. Strasser, *Top. Catal.* **49**, 241-250 (2008).
21. U. A. Paulus, A. Wokaun, G. G. Scherer, T. J. Schmidt, V. Stamenkovic, N. M. Markovic, P. N. Ross, *Electrochim. Acta* **47**, 3787-3798 (2002**)**.
22. V. R. Stamenkovic, B. S. Mun, M. Arenz, K. J. J. Mayrhofer, C. A. Lucas, G. Wang, P. N. Ross, N. M. Markovic, *Nat. Mater.* **6**, 241-247 (2007).
23. E. Arola, C. J. Barnes, R. S. Rao, A. Bansil, P. M, *Surf. Sci.* **249**, 281-288 (1991).
24. N. Toshima, Y. Wang, *Langmuir* **10,** 4574-4580 (1994).
25. R. E. Schaak, A. K. Sra, B. M. Leonard, R. E. Cable, J. C. Bauer, Y.-F. Han, J. Means, W. Teizer, Y. Vasquez, E. S. Funck, *J. Am. Chem. Soc.* **127,** 3506-3515 (2005).
26. B. Lim, M. Jiang, P. H. Camargo, E. C. Cho, J. Tao, X. Lu, Y. Zhu, Y. Xia, *Science* **324**, 1302-1305 (2009).
27. G. Chen, D. Xia, Z. Nie, Z. Wang, L. Wang, L. Zhang, and J. Zhang, *Chem. Mater.* **19***,* 1840-1844 (2007)
28. C. B. Murray, C. R. Kagan, M. G. Bawendi, *Annu. Rev. Mater. Sci.* **30**, 545-610 (2000).
29. Y. Xiong, Y. Xia, *Adv. Mater.* **19,** 3385-3391 (2007).
30. J. Zhang, K. Sun, A. Kumbhar, J. Fang, *J. Phys. Chem. C* **112**, 5454 -5458 (2008).
31. Z. L. Wang, *J. Phys. Chem. B* **104**, 1153-1175 (2000).